ORIGINAL ARTICLE

Centimeter-level clock synchronization and space-borne timescale generation for BDS-3 using inter-satellite link measurements

Jianhua Yang[1,2] · Chengpan Tang[1] · Xiaogong Hu[1] · Shanshi Zhou[1] · Li Liu[3] · Yezhi Song[1] · Yufei Yang[3] · Rui Guo[3] · Shuai Liu[3] · Junyang Pan[1]

Abstract

Because modernized global navigation satellite systems (GNSSs) carry high-performance atomic clocks onboard, a new problem has arisen regarding whether the clock estimation approach is good enough to reflect the true performance of onboard atomic clocks. This paper proposes a new and novel centimeter-level clock synchronization approach for BDS-3 satellites based on two-way comparisons using inter-satellite link measurements. The proposed approach estimates satellite clock offsets by adjusting satellite clock offsets obtained from inter-satellite ranging measurements, and measurement noise is greatly reduced. The noise level of clock offsets estimated by the new approach is 0.7 cm, which is 41% of that of clock offsets estimated by ISL direct two-way comparisons. Compared to the ODTS approach, the new approach efficiently eliminates orbit errors in clock offsets. On this basis, the paper presents a space-borne timescale (SPBT) using high-performance atomic clocks onboard BDS-3 satellites. The frequency stability of the SPBT is 8.6E-16 at a 1-day interval; this result is superior to ground GNSS timescales such as BDT. Based on the SPBT, this paper evaluates the performance of the BDS-3 onboard atomic clock. The 2-h and 24-h prediction uncertainties for the BDS-3 PHM are 0.04 and 0.12 m, and the frequency stabilities are 1.6e-14 and 3.4e-15 at 10,000-s and 1-day intervals, respectively. The 2-h and 24-h prediction uncertainties of the BDS-3 RAFSs are 0.05 and 0.37 m, and the frequency stabilities are 1.9E-14 and 8.1E-15 at 10,000-s and 1-day intervals. This study contributes to autonomous navigation and signal-in-space accuracy improvements for GNSSs.

Keywords Inter-satellite link · Satellite clock offsets · Onboard atomic clocks · Timescale · BDS-3 · Space-borne passive hydrogen maser

1 Introduction

Satellite onboard atomic clocks are essential instruments for global navigation satellite systems (GNSSs) since GNSSs measure time and distance by comparing clocks. The performance of satellite clocks and the accuracy of their offset estimation are critical factors in the modeling and prediction of satellite clock offsets based on the broadcasted information. Therefore, the standard point positioning accuracy is

✉ Chengpan Tang
  cptang@shao.ac.cn

  Jianhua Yang
  yangjianhua@shao.ac.cn

  Xiaogong Hu
  hxg@shao.ac.cn

  Shanshi Zhou
  sszhou@shao.ac.cn

  Li Liu
  lliu@shao.ac.cn

  Yezhi Song
  syz@shao.ac.cn

  Yufei Yang
  gnssyyf@163.com

  Rui Guo
  guorui@shao.ac.cn

  Shuai Liu
  liushuai0810@sina.com

  Junyang Pan
  panjy@shao.ac.cn

[1] Shanghai Astronomical Observatory, Chinese Academy of Science, No. 80 Nandan Road, Shanghai 200030, China

[2] University of Chinese Academy of Sciences, No. 19 Yuquan Road, Beijing 100049, China

[3] Beijing Satellite Navigation Center, No. 22 Beijing Road, Beijing 100094, China

directly affected by them. Broadcast clock parameter errors dominated the signal-in-space ranging errors (SISREs) of early GPS satellites, such as the BLOCK IIA and BLOCK IIR and GLONASS satellites (Warren and Raquet 2003; Montenbruck 2015a; Yang et al. 2021). Due to the irregular behaviors of onboard atomic clocks, clock offsets are difficult to precisely model and predict at the centimeter level. Hence, developing a real-time clock estimation approach that can handle real-time problems with minimal computational burden and fewer quality control issues is imperative. This approach would be ideal for achieving real-time precise point positioning (Hauschild and Montenbruck 2009; Ge et al. 2012).

New emerging systems, such as BDS-3 in China and Galileo in Europe, as well as The Global Positioning System (GPS), employ highly stable onboard atomic clocks. A modernized GPS employs several cesium atomic clocks with high long-term frequency stability both on the ground and satellite to together maintain the time standard of the system together and uses several rubidium atomic clocks with high short-term frequency stability as the main payload for PNT services (Montenbruck et al. 2017; Wang et al. 2017b). BDS-3 and Galileo employ multiple RAFSs and PHMs as the key elements of the navigation payload (Droz et al. 2009, 2010; Steigenberger and Montenbruck 2016; Wu et al. 2018; Kouba 2019).

A new problem has arisen regarding whether the clock estimation approaches are accurate enough to obtain the true clock offsets. With an ideal clock offsets estimation approach, the estimation errors are a small part of the detrended clock residuals, or irregular variations in the onboard clock outputs dominate the detrended clock residuals. The most commonly used satellite clock estimation approach is ODTS (The Orbit Determination and Time Synchronization), which simultaneously estimates satellite clock offsets and orbit parameters using pseudorange and carrier-phase measurements from a globally distributed network. ODTS is compatible well with the OCX of GPS, Galileo and IGS analysis centers (Dow et al. 2007; Bertiger et al. 2010; Steigenberger and Montenbruck 2016; Johnston et al. 2017). However, due to the high correlations between orbit and clock parameters and solar pressure modeling errors, the estimated clock offsets contain periodic orbit errors at several centimeters to decimeter level (Montenbruck et al. 2015b; Tang et al. 2016; Zhou et al. 2016). Periodical orbit errors degrade the performance of the apparent clock offsets, and as a result advantage of the high stability of the atomic clocks onboard of GPS and Galileo cannot be fully exploited. Periodical orbit errors in clock solutions from ODTS increase the deviation of the clock solutions from the quadratic polynomial model and degrade the broadcast clock parameter accuracy. Thus, the ODTS method may not be a sufficiently accurate approach.

Compared to atomic clocks onboard BDS-2 satellites, with stabilities comparable to those of GPS Block IIR satellites (Zhou et al. 2016), BDS-3 satellites are equipped with PHMs or rubidium atomic clocks. The stabilities of highly stable rubidium atomic clocks and PHMs are superior to those of BDS-2 satellites. The early BDS-2 satellites are equipped with atomic clocks that have performance comparable to those of GPS Block IIR satellites. Furthermore, BDS-3 satellites are equipped with passive hydrogen maser (PHM) or rubidium atomic clocks. The stabilities of PHMs are expected to be at the same level as those onboard Galileo.

A different clock estimation approach with two-way comparisons is adopted for BDS satellites. By directly comparing two-way measurements, the satellite orbit errors, station coordinate errors, and propagation delay modeling errors are easily eliminated. Two-way comparisons reflect the physical characteristics of the onboard atomic clocks (Liu et al. 2009; Zhou et al. 2016; Pan et al. 2018; Tang et al. 2018). The clock offsets of BDS-2 satellites are measured through L-band two-way satellite time and frequency transfer (TWSTFT). TWSTFT measures the satellite clock offset relative to the information from a ground station (the master station, which keeps BDT) by comparing the L-band uplink pseudorange with the L-Band downlink pseudorange. BDS-3 satellites are equipped with inter-satellite link (ISL) terminals. The ISL facilities enable time-division multiple access (TDMA) and dual, one-way measurements. Relative clock offsets can also be obtained from direct ISL comparisons. Tang et al. (2018) found that directly compared ISL clock offsets exhibit more minor fluctuations than L-band TWSTFT clock offsets, indicating that the direct ISL comparisons are more accurate for clock estimation. Although clock offsets from two-way comparisons are free of orbit errors, they are influenced by measurement noise. In fact, the ISL measurement noise level can reach 10 cm, which is one to two orders of magnitude larger than that of phase measurements. Hence, a direct ISL comparison may not be sufficiently accurate (Wu et al. 2018).

This paper focuses on high-performance atomic clocks onboard BDS-3 satellites and the benefits of these clocks. However, both periodical errors and random noises induced by the clock estimation approach degrade the apparent clock behavior. A new satellite clock estimation (clock synchronization) approach based on ISL measurement adjustment is proposed, and the estimated clock offsets are both free of satellite orbit errors and two-way comparison measurement noise. The proposed approach takes full advantage of redundant observations in ISL measurements to suppress ISL measurement noise and achieves centimeter-level clock synchronization among satellites.

Both GPS and Galileo use ODTS approaches in broadcast satellite clock offset estimation. Apparent orbital variations are present in the estimated clock offsets, further increasing uncertainties in clock prediction (Yang et al. 2021). For

the high-performance atomic clocks onboard modernized GNSS satellites such as PHM clocks of BDS-3 and Galileo satellites, irregular variations of the clock itself are rather small, and the periodic orbit errors dominate the detrended residuals. Frequent update is needed to represent the periodic orbit errors if high signal-in-space accuracy is the goal. The clock parameter errors will dominate the SISRE without frequent updates. However, one should note that frequent updates are an intensive task for the ground control. On the other hand, the broadcasted satellite clock offsets of BDS-3 are generated using L-band two-way comparisons and direct ISL two-way comparisons in combination. The fluctuations and measurement noise in both direct two-way comparisons result in inconsistencies between the estimated clock offsets and in larger errors in broadcasted satellite clock parameters. According to Chen et al. (2020), the BDS-3 broadcasted clock parameter error is 0.57 ns, which dominates the SISRE for BDS-3. In this paper, a new centimeter-level clock synchronization approach is proposed to improve the broadcast clock offset prediction accuracy and reduce the frequency of updates.

The broadcasted satellite clock parameters of GNSSs are referenced to their respective ground system time. The BDS satellite clock parameters are referenced to the BDS Time, with daily stability at 1.3E-14 level (Han et al. 2021). The Galileo satellite clock parameters are referenced to the Galileo precise timing facility-maintained GST, with daily stabilities ranging from 1.1E-15 to 2.7E-15 (Proia et al. 2014). GPS satellite clock parameters are referenced to the GPST. The frequency stability of GPST can reach 7.0E-15 and 2.2E-15 at 10,000-s and 1-day intervals, respectively (Senior and Coleman 2017). Generating a space-borne timescale (SPBT) comparable to the ground-based time scale will benefit GNSS operation and scientific tasks. For GNSS operation, with a highly stable SPBT, the satellites can update the broadcast clock parameters themselves using the inter-satellite link, reducing the frequency of regular updating operations performed by ground control facilities and reducing system operation reliance on the ground segment facilities (Wang et al. 2011, 2017a). High-stability SPBTs will also benefit scientific tasks and programs such as the Atomic Clock Ensemble in Space (ACES) program proposed by the ESA for testing the fundamental laws of physics in space (Cacciapuoti and Salomon 2011) and the future Kepler constellation for reference frame generation (Giorgi et al. 2019; Glaser et al. 2020). It is also possible for BDS-3 to construct a space-borne timescale that is comparable with the ground timescale using the BDS-3 onboard clock only with centimeter clock synchronization results. Once the space-borne timescale is generated, the satellite clock parameters are generated autonomously.

The paper is organized as follows: In Sect. 2, a centimeter-level clock synchronization approach for satellites based on BDS-3 ISL measurement adjustment is introduced promising accuracy improvements. A space-borne timescale is generated, and stability analysis of SPBT is performed in Sect. 3. The space-borne timescale and ISL adjustment clock offsets are used to evaluate the performance of satellite clocks in Sect. 4. Finally, conclusions and discussion are given in Sect. 5.

2 Centimeter-level clock synchronization approach

2.1 Algorithm

Tang et al. (2018) gave basic observation equations for dual, one-way ISL as follows:

$$
\begin{aligned}
\rho_{AB}(t_1) =& \left| \vec{R}_B(t_1) - \vec{R}_A(t_1 - \Delta t_1) \right| + c(clk_B(t_1) - clk_A(t_1) \\
&+ \tau_A^{Send} + \tau_B^{Rcv}) + \Delta\rho_{cor}^{AB} + \zeta_{AB} \\
\rho_{BA}(t_2) =& \left| \vec{R}_A(t_2) - \vec{R}_B(t_2 - \Delta t_2) \right| + c(clk_A(t_2) - clk_B(t_2) \\
&+ \tau_A^{Rcv} + \tau_B^{Send}) + \Delta\rho_{cor}^{BA} + \zeta_{BA}
\end{aligned}
\tag{1}
$$

Satellite B receives pseudorange $\rho_{AB}(t_1)$ from satellite A at time t_1, and satellite A receives pseudorange $\rho_{BA}(t_2)$ from satellite B at t_2. The ISL of BDS-3 follows a time-division multiple access (TDMA) structure. The ISL dual one-way pseudoranges are in general measured at different times. $\vec{R}_A$ and $\vec{R}_B$ are three-dimensional position vectors for satellite A and satellite B, respectively; clk_A and clk_B are the clock offsets of satellite A and B, respectively; c is the speed of light; Δt_1 and Δt_2 are the travel times of light, respectively; τ_A^{Send} and τ_B^{Send} are the hardware delays of satellite A and satellite B in transmittance; τ_A^{Rcv} and τ_B^{Rcv} are the receiving hardware delays of satellite A and satellite B, the hardware delays can be calibrated and removed based on the proposal from Pan et al. 2018; ζ_{AB} and ζ_{BA} are the measurement errors of the ISL; $\Delta\rho_{cor}^{AB}$ and $\Delta\rho_{cor}^{BA}$ are the error corrections for the dual, one-way observations of both satellites, which can be accurately modeled. The error corrections include satellite phase center corrections and relativistic effect corrections.

t_1 and t_2 are different epochs. To obtain clock offsets between two satellites, it is necessary to reduce the dual, one-way observations from different epochs to the same epoch; the corresponding equations are given as follows:

$$\rho_{AB}(t_0) = \rho_{AB}(t_1) + d\rho_{AB} = \left|\vec{R}_B(t_0) - \vec{R}_A(t_0)\right| + c(clk_B(t_0)$$
$$-clk_A(t_0) + \tau_A^{Send} + \tau_B^{Rcv}\big) + \Delta\rho_{cor}^{AB} + \zeta_{AB}$$
$$\rho_{BA}(t_0) = \rho_{BA}(t_2) + d\rho_{BA} = \left|\vec{R}_A(t_0) - \vec{R}_B(t_0)\right| + c(clk_A(t_0)$$
$$-clk_B(t_0) + \tau_A^{Rcv} + \tau_B^{Send}\big) + \Delta\rho_{cor}^{BA} + \zeta_{BA} \qquad (2)$$

where $d\rho_{AB}$ and $d\rho_{BA}$ are the reduction corrections from observation epochs t_1 and t_2 to the target epoch t_0. These variables are related to the differences in the distances and clock offsets of the two satellites from observed epochs to the target epoch. $d\rho_{AB}$ and $d\rho_{BA}$ are given as follows:

$$d\rho_{AB} = \left|\vec{R}_B(t_0) - \vec{R}_A(t_0)\right| - \left|\vec{R}_B(t_1) - \vec{R}_A(t_1 - \Delta t_1)\right|$$
$$- c(clk_B(t_1) - clk_A(t_1)) + c(clk_B(t_0) - clk_A(t_0))$$
$$d\rho_{BA} = \left|\vec{R}_B(t_0) - \vec{R}_A(t_0)\right| - \left|\vec{R}_B(t_2) - \vec{R}_A(t_2 - \Delta t_2)\right|$$
$$- c(clk_A(t_2) - clk_B(t_2)) + c(clk_A(t_0) - clk_B(t_0))$$
$$(3)$$

where $d\rho_{AB}$ and $d\rho_{BA}$ can be calculated from the predicted satellite orbit and clock offset parameters. From Eq. 3, the calculation accuracy of $d\rho_{AB}$ and $d\rho_{BA}$ depends on the accuracies of the satellite clock rate and satellite orbit velocity rather than the satellite position accuracy and predicted clock offset accuracy. According to Tang et al. (2018), time differences between the target epoch and observation epochs are below 3 s, the prediction uncertainty of the BDS-3 satellite velocity is below 0.1 mm/s and the prediction error of the BDS-3 satellite clock rate is below 1.0E-4 ns/s. Therefore, we can calculate that the accuracy loss for $d\rho_{AB}$ and $d\rho_{BA}$ is smaller than 3 mm, which is far less than the current estimation errors for the satellite orbit and clock offset.

By subtracting the reduced, dual, one-way observations in Eq. 2 at the target epoch, the satellite orbit information can be eliminated, and the observation equation for inter-satellite clock offset can be obtained as follows:

$$\frac{\rho_{AB}(t_0) - \rho_{BA}(t_0)}{2} = c[clk_B(t_0) - clk_A(t_0)] + \frac{\zeta_{AB} - \zeta_{BA}}{2}$$
$$+ c\left(\frac{\tau_A^{Send} - \tau_A^{Rcv}}{2} - \frac{\tau_B^{Send} - \tau_B^{Rcv}}{2}\right)$$
$$+ \frac{\Delta\rho_{cor}^{AB} - \Delta\rho_{cor}^{BA}}{2} \qquad (4)$$

$\Delta\rho_{cor}^{AB}$ and $\Delta\rho_{cor}^{BA}$ can be easily modeled, and the hardware delays are constant values. By subtracting the mentioned variables from the left side of Eq. 4, the inter-satellite clock offset can be obtained by the following equation:

$$c \cdot [clk_B(t_0) - clk_A(t_0)] + \frac{\zeta_{AB} - \zeta_{BA}}{2}$$

$$= \frac{\rho_{AB}(t_0) - \rho_{BA}(t_0)}{2} - c\frac{\tau_A^{Send} - \tau_A^{Rcv}}{2} + c\frac{\tau_B^{Send} - \tau_B^{Rcv}}{2}$$
$$- \frac{\Delta\rho_{cor}^{AB} - \Delta\rho_{cor}^{BA}}{2} \qquad (5)$$

The inter-satellite clock offsets obtained by Eq. 5 are referred to as Ka-band inter-satellite direct clock offsets. While Ka-band inter-satellite direct clock offsets are free of orbital errors, they suffer from ISL measurement errors, including systematic errors and random noise. Tang et al. (2018), Pan et al. (2018) and Chen et al. (2020) analyzed the characteristics of the Ka-band inter-satellite direct clock offsets and used them to determine satellite clock offsets relative to BDT. Random noise at the 10-cm level and periodic fluctuations were observed from the Ka-band inter-satellite direct clock offsets. Previous studies used Ka-band inter-satellite direct clock offsets as input measurements for BDS-3 broadcast clock parameter generation.

The BDS-3 ISL has a TDMA structure. One satellite connects with different satellites in different time intervals to perform dual, one-way ranging measurements. In one connectivity cycle whose duration is 60 s, multiple Ka-band inter-satellite direct clock offsets between the clocks of one specific satellite and the other satellite can be obtained by processing measurements using Eq. 5. Therefore, many redundant Ka-band inter-satellite direct clock offsets are given for clock offset estimation. For example, the BDS-3 constellation consists of 30 satellites. Twenty-nine Ka-band inter-satellite direct clock offsets are sufficient for clock synchronization and the estimation of all the satellite clock offsets relative to that of a chosen reference satellite. If N Ka-band inter-satellite direct clock offsets can be obtained in one period for one specific satellite clock (for BDS-3 satellite, N is usually from 10 to 15 within one connectivity cycle), $N*30/2 = N*15$ clock differences in total are present for satellite clock offset estimation. If $N > 2$, redundant Ka-band inter-satellite direct clock offsets can be used to filter the ISL measurement errors.

In the proposed clock estimation approach, least square estimation is used to suppress and filter the ISL measurement errors. The observations of least square estimation are the inter-satellite direct satellite clock offsets in one ISL cycle obtained by processing ISL measurements with Eqs. 1–5. Clock offsets for a specific satellite during an ISL cycle are treated as linear polynomial model including the satellite clock offset at the starting point (a0) of an ISL cycle and a clock rate (a1). The satellite-specific clock model parameters including a0 and a1 relative to a reference satellite are estimated from the ISL clock differences using least-square adjustment. By using least-square estimation, the ISL measurement errors are effectively filtered, and the estimated clock offsets are more precise. Since the Allan deviation of
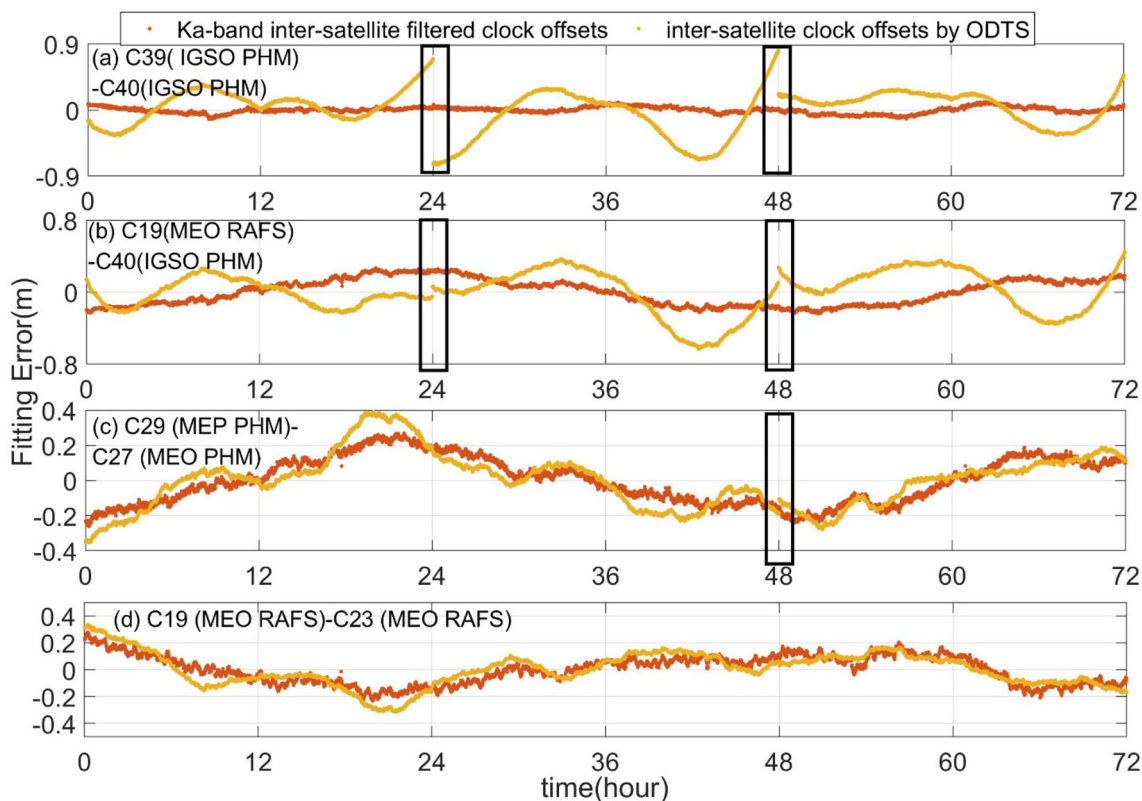
Fig. 1 Satellite clock offset differences for Ka-band inter-satellite filtered clock offsets and precise GFZ products

BDS-3 satellite atomic clocks is below 3e-12 at 60-s averaging interval, the RMS of the accuracy loss caused by such an assumption is below 3 mm. The estimated clock offsets at the starting point (a0) of an ISL cycle are used for analysis in the following context.

In the following context, the estimated clock offsets are referred to as Ka-band inter-satellite filtered clock offsets. Notably, in the proposed algorithm, the clock offset estimations are free of orbit errors. Furthermore, the ISL measurement noises are greatly suppressed.

2.2 Accuracy evaluation

The accuracy of the Ka-band inter-satellite filtered clock offsets will be evaluated in this section. They are first compared with precise clock offsets provided by the GFZ MGEX analysis center. The GFZ precise clock offsets are generated using the ODTS process based on pseudorange and carrier-phase measurements from small numbers (for IGSO) to hundreds (MEO) of globally distributed stations. The clock accuracy of the MGEX GFZ products is 10 cm for BDS-2 (Steigenberger and Montenbruck 2019). Currently, the accuracy of BDS-3 clock offsets has yet to be estimated. In this paper, the accuracy of BDS-3 satellite clock offsets is set at the same level as that of BDS-2.

We take the Ka-band inter-satellite clock offsets of C39–C40 (IGSO–IGSO), C39–C19 (MEO-IGSO), C29–C27 (MEO in the same orbital plane), and C19–C23 (MEO in the different orbital plane) as examples. After removing the same trend, the residuals of GFZ inter-satellite clock offsets and Ka-band inter-satellite filtered clock offsets are compared, as shown in Fig. 1. The red lines are detrended Ka-band inter-satellite filtered clock offset residuals. The orange lines are detrended ODTS clock offset residuals. For the pairs containing IGSO satellites indicated in Fig. 1a and b, the detrended residuals of GFZ precise clock offsets behave quasi-periodically with some inter-day discontinuities, both most probably due to correlation with the uncertainties in the orbit modeling. However, quasi-periodic fluctuations and daily discontinuities are absent in the Ka-band inter-satellite filtered clock offsets. The detrended residuals of Ka-band inter-satellite filtered clock offsets appear as a continuous line in Fig. 1a and b. For MEO, the STD of the detrended Ka-band inter-satellite filtered clock offset is 0.13 m in Fig. 1c and 0.10 m in Fig. 1d, and the STD of the detrended GFZ inter-satellite clock offset is 0.15 m in Fig. 1c and 0.12 m in Fig. 1d. It means the detrended Ka-band inter-satellite filtered clock offsets fluctuate slightly less than the detrended GFZ clock offset differences on the 3-day scale.
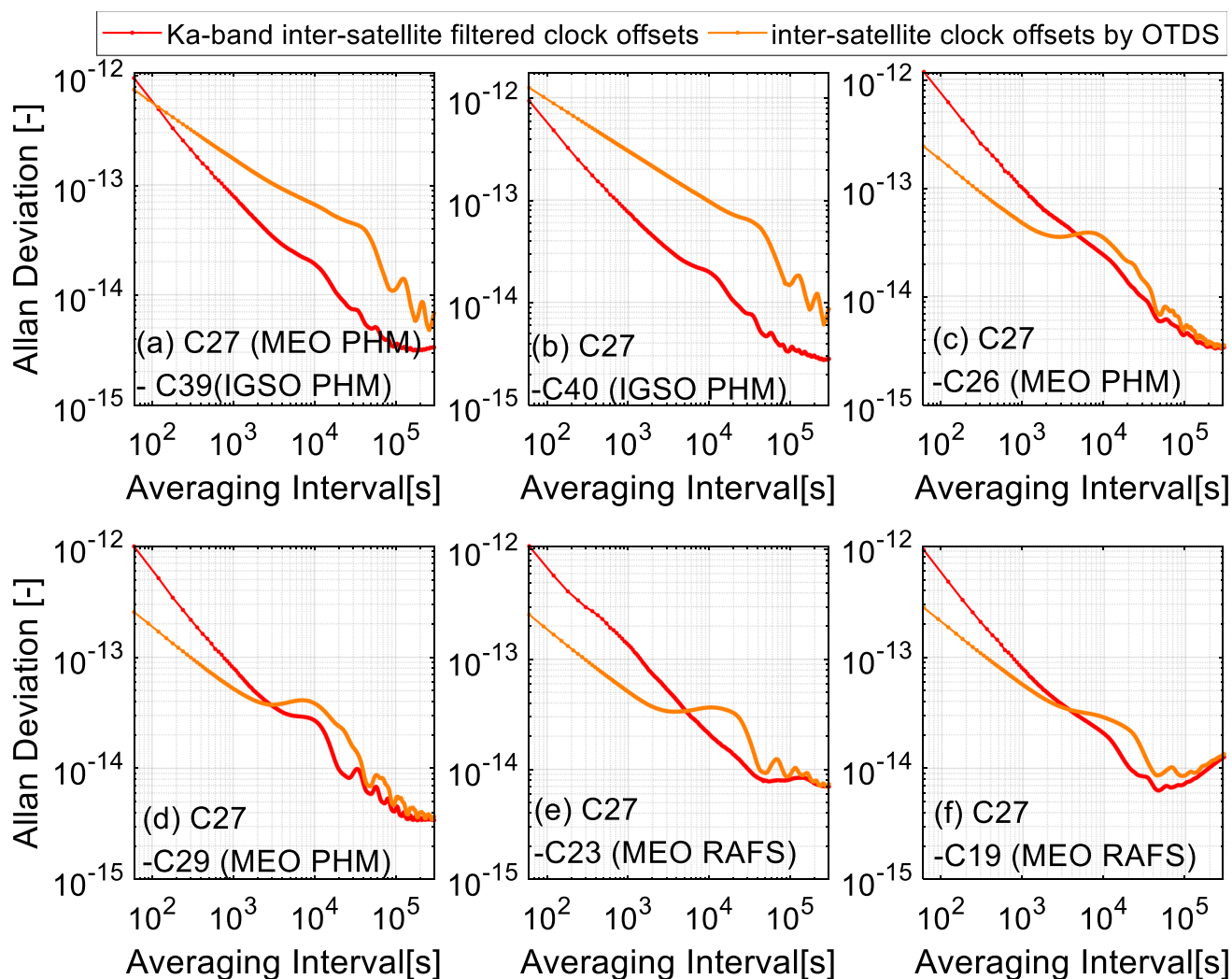
Fig. 2 Frequency stability of GFZ ODTS clock offset differences and LSQ Ka clock offset differences

As shown in Fig. 1, the quasi-periodic variation for the IGSO satellites is more significant than that for MEO satellites, probably indicating a more considerable orbit modeling deficiency in GFZ solutions. Ka-band inter-satellite filtered clock offsets behave more stably compared to both types of satellites. One should note that the frequency instability of the Ka-band inter-satellite filtered MEO satellite clock offsets is larger than that of the GFZ clock solutions with averaging interval of less than 3600 s, as indicated in Fig. 2, since the random noise level of the Ka-band inter-satellite filtered clock offsets are larger than clock offsets generated using carrier phase measurements. However, Ka-band inter-satellite filtered clock offsets display better frequency stability at intervals larger than 3600 s, especially for IGSO satellites. Furthermore, daily discontinuities are found in the GFZ precise clock offsets due to the different arc data involved, and the Ka-band inter-satellite filtered clock offsets are continuous at day boundaries.

Considering that it is difficult for BDS-3 to deploy monitoring stations worldwide, the clock offsets estimated by the new approach are more suitable for BDS to generate clock parameters than the cock offsets estimated by the ODTS method.

The Ka-band inter-satellite direct clock offsets and Ka-band inter-satellite filtered clock offsets are compared in Fig. 3. The blue lines indicate the detrended residuals of Ka-band inter-satellite direct clock offsets, which are estimated by the Ka-band ISL two-way comparison approach (3 s intervals). The red lines indicate the detrended residuals of Ka-band inter-satellite filtered clock offsets.

From Fig. 3, the Ka-band inter-satellite filtered clock offsets not only can directly estimate inter-satellite clock offset when ISLs are not established directly, but also suffer from less noise and lower estimation errors.
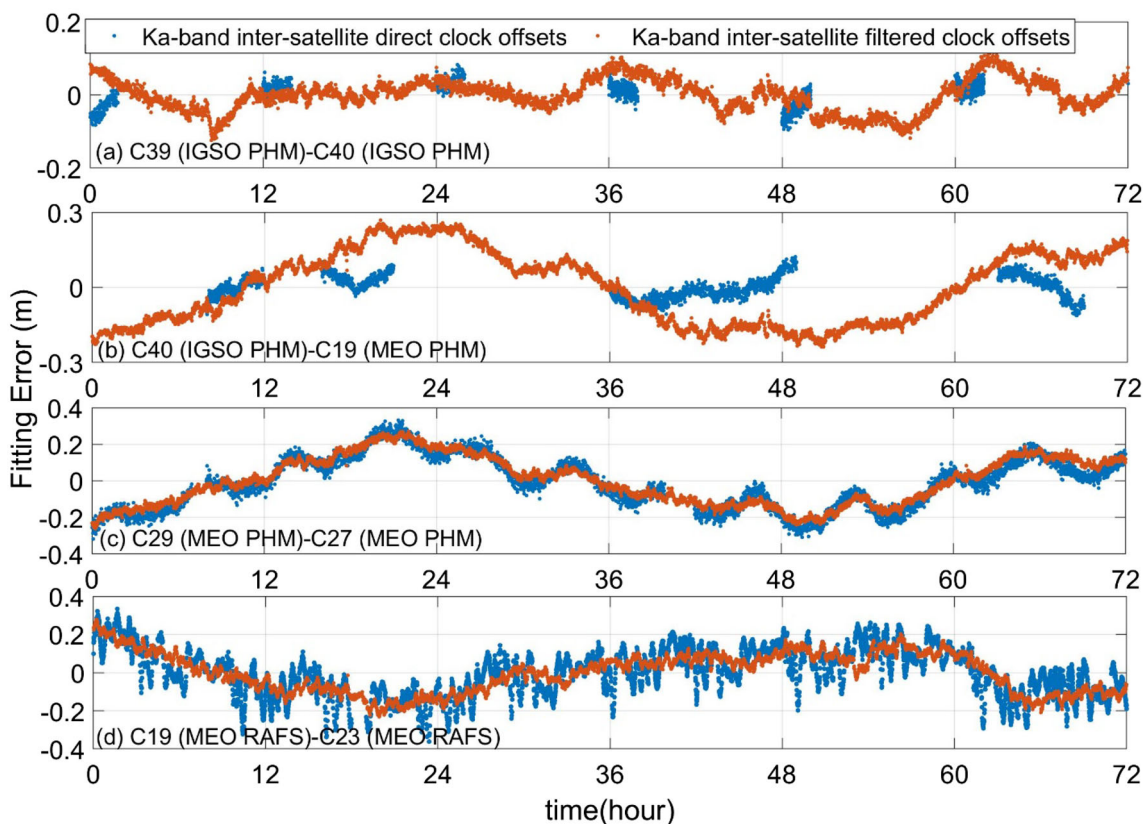
Fig. 3 Three-day detrended residuals of Ka-band inter-satellite filtered clock offsets and Ka-band inter-satellite direct clock offsets
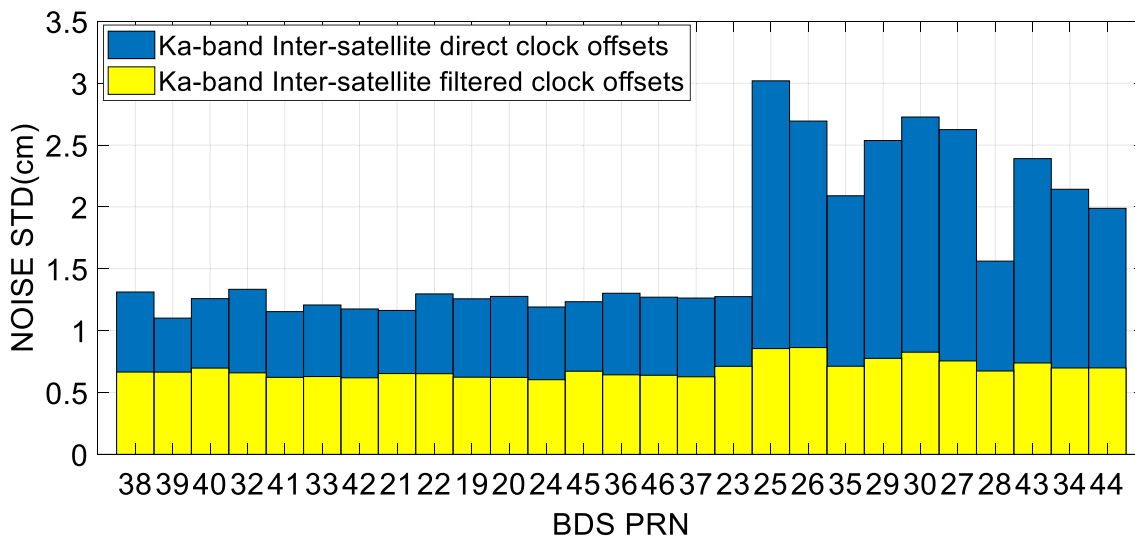

Fig. 4 Clock offset noise level for the two methods

Linear polynomial fitting was performed every 10 min for Ka-band inter-satellite direct clock offsets and Ka-band inter-satellite filtered clock offsets. The STD results of the fitting residual were calculated for each inter-satellite clock offset sequence. Averaging the STD results of each ISL for 10 days, the noise STD of each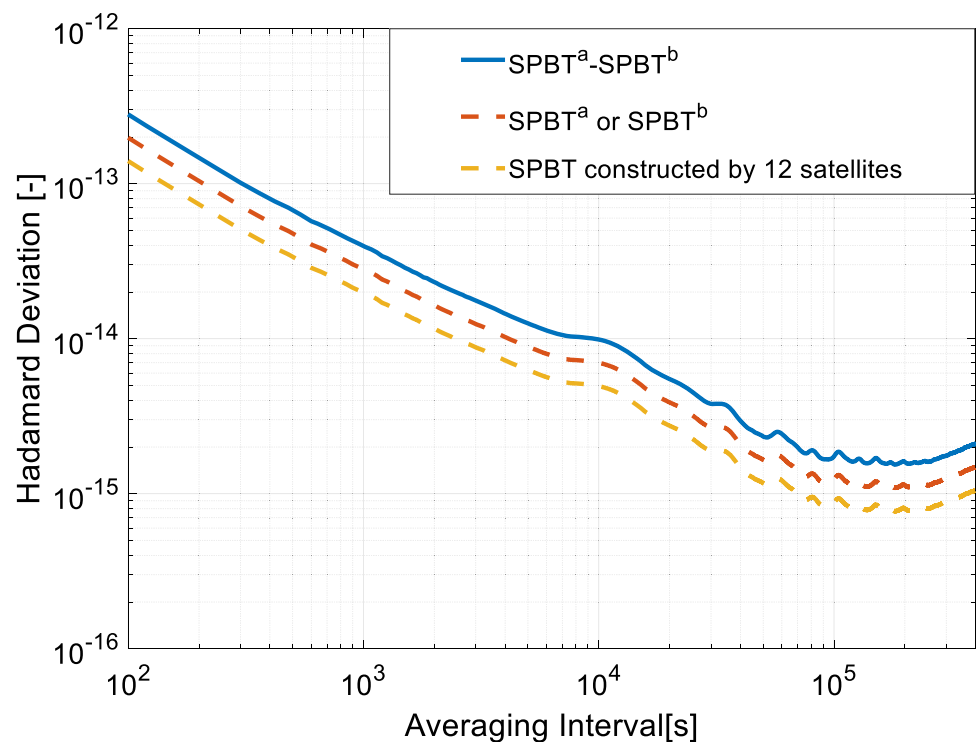 ISL was obtained. Selecting a satellite clock and further averaging the noise STD of ISLs only containing the selected satellite clock, the averaged noise STD of the selected satellite clock was obtained. The noise levels (STD) of Ka-band inter-satellite direct clock offsets (blue) and Ka-band inter-satellite filtered clock offsets (yellow) are given in Fig. 4. Obvious difference for blue bars dividing

Table 1 The SPBT information

PRN	Overlapping Hadamard deviation (1 day)	Weight	Clock cluster
C41	1.89E−15	0.40	$SPBT^a$
C28	2.50E−15	0.21	
C45	2.95E−15	0.16	
C35	3.47E−15	0.12	
C26	4.10E−15	0.01	
C34	8.46E−15	0.02	
C40	1.97E−15	0.37	$SPBT^b$
C27	2.40E−15	0.24	
C29	3.44E−15	0.13	
C46	3.25E−15	0.13	
C37	3.95E−15	0.08	
C36	4.12E−15	0.04	

3 Generation of BDS-3 space-borne timescale

Since high-performance PHMs on BDS-3 satellites are relatively stable, it is possible to generate a space-borne timescale that is comparable with the ground timescale (i.e., BDT) in terms of frequency stability. After a space-borne timescale is generated, the broadcasted clock parameters can be autonomously updated onboard. This section concentrates on the feasibility of generating a space-borne timescale using Ka-band inter-satellite filtered clock offsets of high-performance atomic clocks onboard BDS-3 satellites.

3.1 Generation method

A space-borne timescale is generated as the weighted average of satellite clock offsets. Unlike the timescale in the ALGOS approach (Weiss and Weissert 1991; Gao et al. 2008), which is used for real-time applications, a space-borne timescale is generated in a postprocessing mode for feasibility analysis and performance assessment. The inputs for the space-borne timescale generation are the Ka-band inter-satellite clock offsets with respect to a chosen reference satellite clock. The space-borne timescale is usually expressed based on the corresponding difference to a reference satellite clock.

at PRN = 25 is probably related to satellite manufacturers (The satellites before PRN = 25 in Fig. 4 are manufactured by CAST, and the rest are manufactured by SECM).

From Fig. 4, the noise level of the clock offsets estimated with the new approach is 0.7 cm, and that of the clock offsets estimated with the two-way comparison method is 1.7 cm. Thus, the noise level of the Ka-band inter-satellite filtered clock offset is 41% of the noise level of the Ka-band inter-satellite direct clock offset.

Fig. 5 Frequency stability of the two SPBT differences

Space-borne timescale generation can be conducted as follows:

$$SPBT(t) - clk_q(t) = \frac{\sum_{i \neq q}^{N} w_i \left(\Delta clk_{iq}^{lsq}(t) \right)}{N} \quad (6)$$

where N is the number of satellites for space-borne timescale generation, q is the reference satellite, i is the subscript of satellite, $\Delta clk_{iq}^{lsq}(t)$ is the inter-satellite clock offset of satellite i with respect to reference satellite q at time t based on the approaches in Sect. 2, $SPBT(t)$ is the generated space-borne timescale at time t, and $clk_q(t)$ is the clock offset of reference satellite q at time t. w_i refers to the weight of satellite i for space-borne timescale generation:

$$\sum w_i = 1 \quad (7)$$

The clock offsets of satellite i with respect to the space-borne timescale can be obtained by:

$$SPBT(t) - clk_i(t) = \left(SPBT(t) - clk_q(t) \right) - \Delta clk_{iq}^{lsq}(t) \quad (8)$$

where $clk_i(t)$ is the estimated clock offset of satellite i at time t and $SPBT(t) - clk_q(t)$ is the estimated difference of space-borne timescales with the reference satellite clock q from Eq. 6.

The space-borne timescale is generated using a two-step process. First, the preliminary SPBT is obtained following Eq. 8 with the same weights: $w_i = \frac{1}{N}$, $(i = 1, 2, 3, \ldots, N)$. All the satellite clock offsets relative to the preliminary SPBT are easily obtained from Eq. 8. The clock offsets relative to the preliminary SPBT are used to calculate the overlapping Hadamard variance of all the satellites. Second, the SPBT is generated using Eq. 6 with adjusted weights. The adjusted weights follow Eq. 9.

$$\omega_i(t) = \frac{\frac{1}{\sigma_i^2}}{\sum_{i=1}^{n} \frac{1}{\sigma_i^2}} \left(\sum_{i=1}^{N} \omega_i(t) = 1, \ \max(\omega_i(t)) < \frac{A}{N} \right) \quad (9)$$

where σ_i^2 is the overlapping Hadamard variance at a 1-day interval, ω_i represents the weights, and A is the empirical parameter associated with maximum weight, which is empirically set to 2.5 (Qin et al. 2018).

The two-step-derived SPBT yields the smallest overlapping Hadamard variance at a 1-day interval among all the onboard satellite clock cases and is the proposed space-borne timescale for satellite clock prediction and evaluation.

Table 2 Performance of SPBT

	2-h prediction error RMS/95% (m)	24-h prediction error RMS/95% (m)	100-s frequency stability	1000-s frequency stability	10,000 s frequency stability	86,400-s frequency stability
$SPBT^a - SPBT^b$	0.023/0.047	0.047/0.096	2.35E−13	3.90E−14	9.88E−15	1.73E−15
$SPBT^a$ or $SPBT^b$	0.016/0.033	0.033/0.068	1.66E−13	2.76E−14	6.99E−15	1.22E−15
$SPBT^c$	0.012/0.024	0.023/0.048	1.18E−13	1.95E−14	4.94E−15	8.64E−16

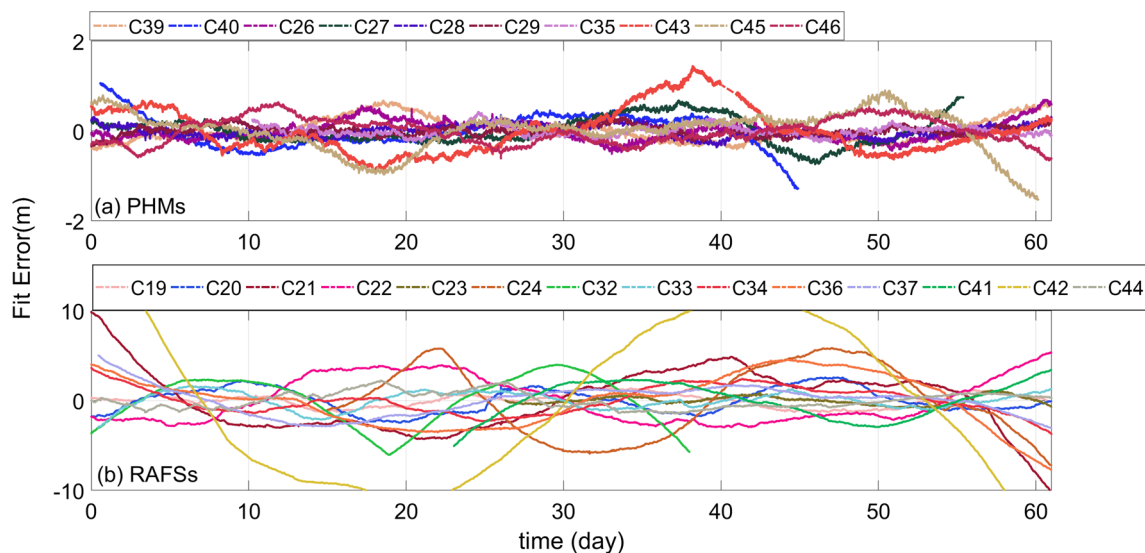**Fig. 6** Sixty-day fitting residuals for onboard atomic clocks: (**a**) PHMS and (**b**) RAFS
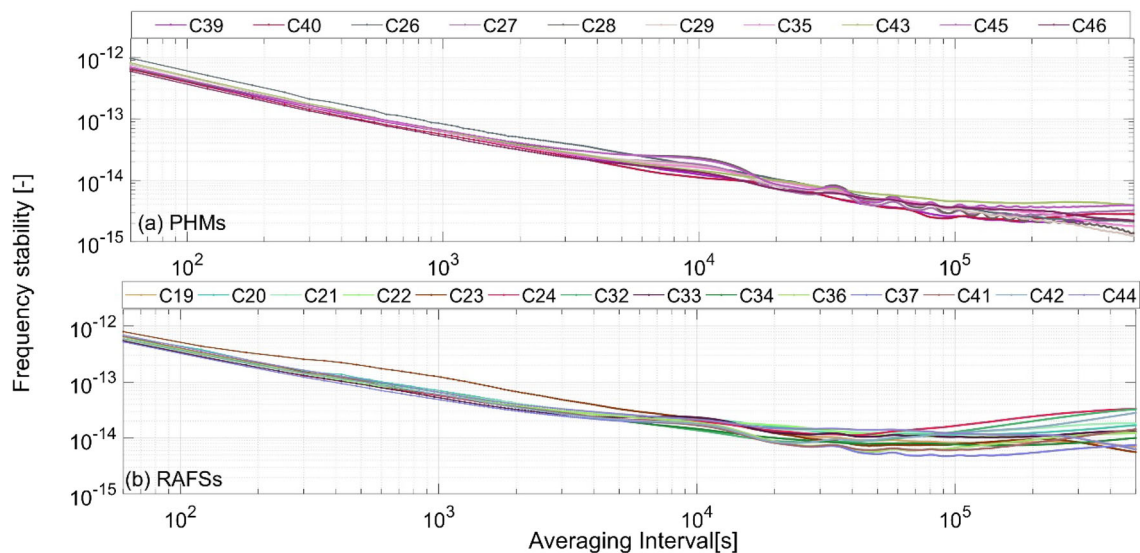

Fig. 7 Frequency stability of BDS-3 onboard atomic clocks

3.2 Performance

In this section, the performance of the space-borne timescale generated as discussed in Sect. 3.1 is evaluated. Given that a space-borne timescale is usually not accessible, the differences between two separate space-borne timescales are used for space-borne timescale performance evaluation.

Frequency and phase changes for onboard atomic clocks will seriously affect the observed apparent clock. After excluding abnormal satellites and epochs, 12 onboard, high-performance atomic clocks are selected to construct a preliminary space-borne timescale. Based on the preliminary space-borne timescale, the overlapping Hadamard deviations

of the 12 selected satellite clocks with 1-day averaging intervals are calculated. The 12 satellite clocks are divided into two separate clusters. Each cluster contains 6 satellites. The average frequency stabilities of the 6 satellites in the two clusters are set to be as equal as possible. Each cluster of satellites is used to generate a space-borne timescale. Therefore, two different space-borne timescales $SPBT^a$ and $SPBT^b$ are generated independently. The overlapping Hadamard deviations of the selected 12 satellites and the weights used to generate the final space-borne timescale are given in Table 1.

By selecting a common onboard atomic clock, the two SPBT differences can be obtained from Eq. 10.:

Table 3 Frequency stability of BDS-3 PHMs

PRN	60 s	10,000 s	86,400 s
C39	6.61E−13	1.24E−14	2.66E−15
C40	6.32E−13	1.08E−14	2.31E−15
C26	9.67E−13	1.72E−14	3.71E−15
C27	7.64E−13	1.81E−14	2.97E−15
C28	6.54E−13	2.31E−14	3.32E−15
C29	7.71E−13	1.68E−14	3.61E−15
C35	7.11E−13	1.60E−14	3.67E−15
C43	8.10E−13	1.43E−14	4.28E−15
C45	6.81E−13	2.19E−14	3.43E−15
C46	5.91E−13	1.35E−14	3.65E−15
Maximum	9.67E−13	2.31E−14	4.28E−15
Minimum	5.91E−13	1.08E−14	2.31E−15
Mean	7.24E−13	1.64E−14	3.36E−15

Table 4 Frequency stabilities of BDS-3 RAFSs

PRN	60 s	10,000 s	86,400 s
C19	5.57E−13	2.04E−14	7.77E−15
C20	6.51E−13	2.24E−14	1.02E−14
C21	5.52E−13	1.98E−14	1.08E−14
C22	5.83E−13	1.98E−14	9.43E−15
C23	7.95E−13	2.22E−14	6.24E−15
C24	5.47E−13	1.98E−14	1.08E−14
C32	5.93E−13	1.37E−14	7.85E−15
C33	5.43E−13	2.34E−14	9.72E−15
C34	6.55E−13	1.46E−14	7.38E−15
C36	6.28E−13	1.89E−14	4.74E−15
C37	5.22E−13	1.72E−14	4.33E−15
C41	6.53E−13	1.69E−14	4.95E−15
C42	5.89E−13	1.78E−14	7.72E−15
C44	6.91E−13	2.14E−14	1.20E−14
Maximum	7.95E−13	2.34E−14	1.20E−14
Minimum	5.22E−13	1.37E−14	4.33E−15
Mean	6.11E−13	1.92E−14	8.14E−15

$$SPBT^a - SPBT^b = \left(SPBT^a - clk_A\right) - \left(SPBT^b - clk_A\right) \tag{10}$$

where A is the selected common onboard atomic clock. The $SPBT^a - clk_A$ and $SPBT^b - clk_A$ can be calculated from Eq. 8.

The prediction uncertainty and the frequency stabilities of the space-borne timescale differences $SPBT^a - SPBT^b$ can be evaluated with Eq. 10. With the assumptions that $SPBT^a$ and $SPBT^b$ are characterized by equal performance and that $SPBT^a$ and $SPBT^b$ are generated separately, the frequency stabilities and prediction errors of the space-borne timescale differences are $\sqrt{2}$ times of a specific timescale, i.e., $SPBT^a$ or $SPBT^b$. The overlapping Hadamard deviation is given in Fig. 5. The blue line denotes the frequency stabilities of $SPBT^a - SPBT^b$, and the red line denotes the frequency stabilities of one specific SPBT (SPBT[a] or SPBT[b]). The frequency stability is obtained by assuming that SPBT[a] and SPBT[b] are characterized by equal performance and that the frequency stability of the space-borne timescale differences is $\sqrt{2}$ times that of one specific timescale, i.e., SPBT[a] or SPBT[b]

The daily frequency stability and 2-h prediction errors (from 0 to 2 h) and 24-h prediction error (from 0 to 24 h) of space-borne timescale differences for $SPBT^a$ and $SPBT^b$ are given in Table 2.

Table 2 shows that the 2-h prediction error of the SPBT is 0.02 m, the 1-day prediction error is 0.07 m, and the frequency stability of the SPBT is 6.99E−15 and 1.22E−15 at 10000-s and 1-day intervals, respectively. These levels are the same as those for GPST and GST. If the number of BDS-3 satellites is increased when constructing the SPBT, the SPBT-based results will be theoretically better than the results of $SPBT^a$ and $SPBT^b$. Assuming $SPBT^a$ and $SPBT^b$ share the same frequency stability, frequency stability of $SPBT^a$ or $SPBT^b$ is $\sqrt{2}$ times of the frequency stability of the SPBT[c], which was generated by all the 12 satellites. Therefore, if all 12 satellites are used to generate the SPBT[c], the frequency stabilities of the SPBT[c] at 10000-s and 1-day intervals are expected to be 4.94E−15 and 8.64E−16, respectively.

4 Performance evaluation of onboard atomic clocks

Having a space-borne timescale with stable frequency is a prerequisite for autonomous broadcast clock parameter generation and performance evaluation of onboard atomic clocks. From Sect. 3, the performance of the obtained space-borne timescale is comparable to that of ground timescales. In this section, at least 6 atomic clocks with the best frequency stability (C26, C28, C29, C39, C43, C45, and C46) are used to generate the SPBT to evaluate the performance of BDS-3 onboard atomic clocks. Because more satellites or better clocks are used to construct SPBT than are used for $SPBT^a$ or $SPBT^b$, the performance results for SPBT are theoretically better than those for $SPBT^a$ or $SPBT^b$.

Table 5 Twenty-four-hour prediction error for BDS-3 PHMs (60 days)

PRN	Fitting degree	RMS (m)	95% error (m)
39	1	0.10	0.21
40	1	0.06	0.12
26	1	0.12	0.25
27	1	0.10	0.20
28	1	0.10	0.21
29	1	0.10	0.19
35	1	0.10	0.20
43	1	0.12	0.24
45	1	0.14	0.30
46	1	0.23	0.45
	MEAN	0.12	0.24

Table 6 24-h prediction error for BDS-3 RAFSs (60 days)

PRN	Fitting degree	RMS (m)	95% error (m)
19	2	0.33	0.74
20	2	0.41	0.91
21	2	0.55	1.28
22	2	0.52	1.15
23	2	0.25	0.56
24	2	0.44	1.00
32	2	0.32	0.58
33	2	0.41	0.85
34	2	0.35	0.68
36	2	0.23	0.51
37	2	0.23	0.49
41	2	0.31	0.64
42	2	0.28	0.62
44	2	0.62	1.53
	MEAN	0.37	0.82

4.1 Frequency stability

The long-term residuals of the clock offsets after removing quadratic polynomial trends reflect the frequency stability behavior in the time domain. With respect to the SPBT, the 60-day quadratic polynomial fitting residuals are shown in Fig. 6.

The average STD value of PHMs is 0.27 m, and the best value is 0.11 m. The average STD value of RAFS is 2.39 m, and the best value is 0.46 m.

Frequency stability is a crucial parameter that describes the ability of an atomic clock to maintain a constant frequency. The value and characteristic of frequency stability at different time scales can reflect the punctuality of the clock

at that particular time scale. As a result, frequency stability is highly correlated with the predictive ability of atomic clocks, and many researchers take it as an important indicator to evaluate the clock's performance (Jia et al. 2019). Figure 7 plots the frequency stability of the BDS-3 satellites.

The statistical results for BDS-3 PHMs are given in Table 3. Similarly, the frequency stabilities of BDS-3 RAFSs are given in Table 4.

The 10000-s and daily frequency stabilities of the BDS-3 PHMs are 1.6E−14 and 3.4E−15. The 10000-s and daily frequency stabilities of the BDS-3 RAFSs are 1.92E−14 and 8.14E−15, respectively. The previously computed daily frequency stabilities obtained by ODTS are 3.8E−15 ~ 6.0E−15 for BDS-3 PHMs (Zhou et al. 2020; Wu et al. 2018). Thus, these results are better than the previously computed values obtained by ODTS (The detailed comparison can refer to Fig. 2).

4.2 Prediction uncertainty

A 24-h prediction is performed by fitting the previous 24-h clock offsets with a linear polynomial model for PHMs and quadratic model for RAFSs. The statistical results for the 60-day prediction error (from 0 to 24 h) are given in Tables 5 and 6.

The average RMS of the 24-h prediction errors for the PHMs is 0.12 m, and the best value is 0.06 m. The prediction errors of C40 from April 1 to April 10 are shown in Fig. 8; the blue line in Fig. 8a is the clock offset based on the spaceborne time scale, the red line in Fig. 8a is the predicted clock offset, the red line in Fig. 8b is the 24-h prediction error, and the blue line in Fig. 8b plots the fitting residuals of the previous 24-h clock offset.

The 24-h prediction uncertainty of the BDS-3 RAFSs is 0.37 m, significantly worse than that of the PHMs; additionally, the best RAFS case is observed for C36, with an error of 0.23 m. Similar to Fig. 8, the prediction errors of C36 from April 1 to April 10 are shown in Fig. 9.

The BDS-3 broadcast clock parameters are updated every hour. The short-term prediction uncertainty, i.e., the 2-h prediction error, is closely related to the BDS-3 signal-in-space ranging error (SISRE) and PNT performance (Yang et al. 2021). The results suggest that if the prediction time and fitting time are both two hours, the prediction uncertainty of the linear fitting model is lower than that of the quadratic polynomial model both for PHM and RAFS clocks. Referring to the SPBTs, the statistics for the short-term (2-h) prediction errors of the PHMs and RAFSs are shown in Tables 7 and 8.

The average RMS value of the 2-h prediction errors of the BDS-3 PHMs is 0.04 m, and the satellite with the best PHM clock is C40, with an error of only 0.03 m. The prediction errors of C40 from April 1 to April 3 are shown in Fig. 10.
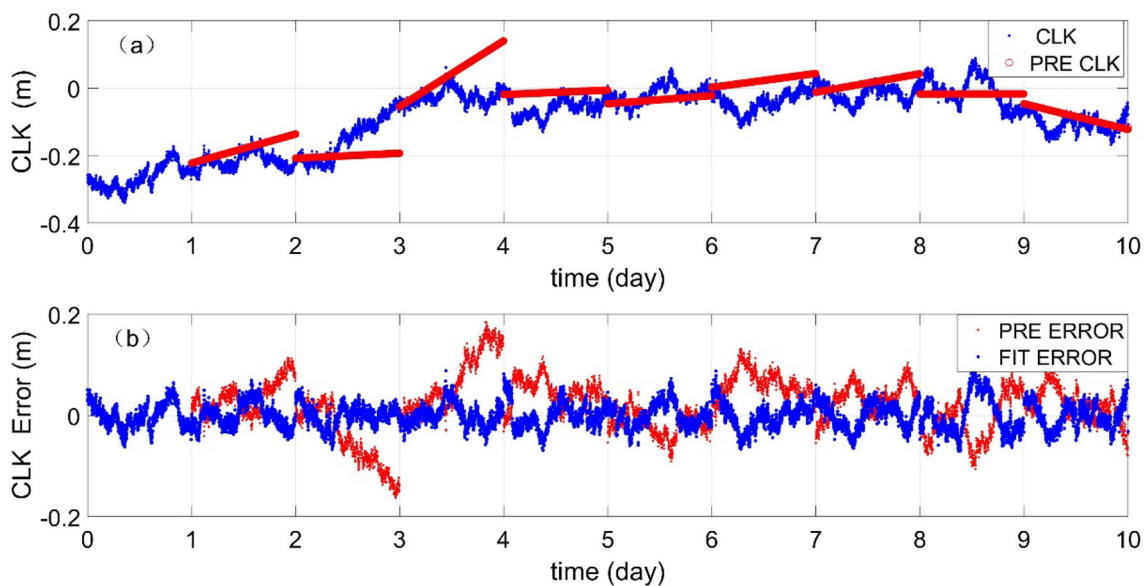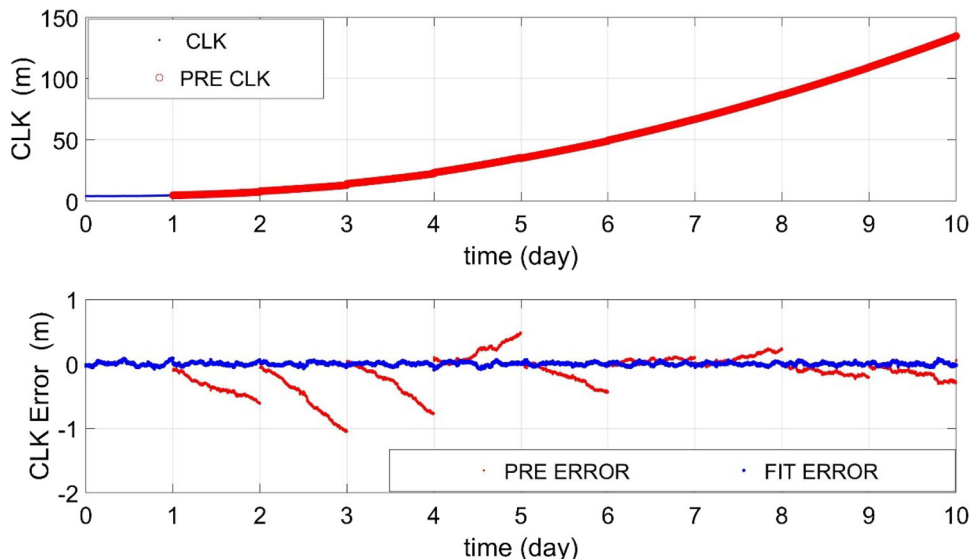
Fig. 8 One-day prediction error for C40 (PHM)

Fig. 9 One-day prediction error for C36 (RAFS)

The average RMS value of the 2-h prediction errors of the BDS-3 RAFSs is 0.05 m. Among them, the satellite with the best RAFS clock is C32, with an error of only 0.04 m. The prediction errors of C32 from April 1 to April 3 are shown in Fig. 11.

By comparison, it can be found that the 2-h predictive ability of PHMs is slightly better than that of RAFSs, but the results are generally similar. The above results are slightly better than the previously published values obtained by ODTS, an example of which may be found in Qin et al. 2019, who reports a 0.08 m error (RMS) for 2-h prediction.

5 Conclusion and discussion

This paper focuses on a feasibility analysis of generating a space-borne timescale stable enough to compete with ground timescales. Basic functions of a space-borne timescale include accurate clock synchronization and the provision of a clock prediction reference. First, this paper proposes a new centimeter-level clock synchronization approach that uses ISL measurements to estimate high-precision inter-satellite clock offsets. Compared to the clock offsets estimated by the ODTS approach, the clock offsets estimated by the new approach do not suffer from daily discontinuities and periodic orbit errors. The new approach can yield more accurate

Table 7 Two-hour prediction errors for the BDS-3 PHMs (60 days)

PRN	Fitting degree	RMS (m)	95% error (m)
C39	1	0.04	0.07
C40	1	0.03	0.05
C26	1	0.06	0.11
C27	1	0.04	0.09
C28	1	0.06	0.11
C29	1	0.04	0.09
C35	1	0.04	0.07
C43	1	0.04	0.08
C45	1	0.05	0.11
C46	1	0.04	0.07
	Mean	0.04	0.09

Table 8 Two-hour prediction errors for the BDS-3 RAFSs (60 days)

PRN	Fitting degree	RMS (m)	95% error (m)
C19	1	0.05	0.11
C20	1	0.06	0.11
C21	1	0.05	0.11
C22	1	0.05	0.10
C23	1	0.06	0.12
C24	1	0.05	0.09
C32	1	0.04	0.09
C33	1	0.05	0.10
C34	1	0.04	0.08
C36	1	0.05	0.10
C37	1	0.04	0.09
C41	1	0.04	0.09
C42	1	0.04	0.09
C44	1	0.06	0.11
	Mean	0.05	0.10

offsets with higher frequency stabilities at averaging intervals from 10,000 s to 1 day. The new approach can obtain inter-satellite clock offsets with a lower noise level of 0.7 cm, which is 41% less than that of the Ka-band inter-satellite two-way direct comparison approach.

With the Ka-band inter-satellite filtered clock offsets, a space-borne timescale called SPBT is generated. Benefitting from the onboard high-performance BDS-3 atomic clock and the centimeter-level clock synchronization approach, the frequency stabilities of the SPBT generated with only 6 BDS-3 satellites are better than 7.0E-15 and 1.2E-15 at 10000-s and 1-day intervals, respectively; these values are close to those of ground GNSS timescales. The frequency stability of the SPBT generated by 12 BDS-3 satellites is expected to be

5.0E-15 and 8.6E-16 for 10000-s and 1-day intervals, respectively.

The onboard performance of BDS-3 atomic clocks is evaluated with reference to the SPBTs. The frequency average stabilities of BDS-3 onboard atomic clocks are 1.8E-14 and 6.2E-15 at 10,000- and 86,400-s intervals, respectively. This result is better than the result based on the direct two-way comparison approach (Zhou et al. 2020; Pan et al. 2021). Notably, the frequency stabilities of the best BDS-3 RAFS are 1.7E-14 and 4.3E-15, and the frequency stabilities of the best BDS-3 PHM are 1.1E-14 and 2.2 E-15. The above results indicate that the stabilities of BDS-3 atomic clocks are at the same levels as other GNSSs (Steigenberger et al. 2016; Li et al. 2019).

Based on the new clock synchronization approach, the 2-h prediction uncertainty of BDS-3 onboard atomic clocks is better than 0.05 m (RMS) with respect to the SPBT. By comparison, ODTS clock prediction uncertainty is about 0.08 m (RMS) for 2-h prediction as reported by Qin et al. 2019.

The above results indicate that it is feasible to generate a space-borne timescale comparable to ground time systems using inter-satellite links and highly stable onboard atomic clocks on BDS-3 satellites. Performance evaluations of BDS-3 onboard satellite clocks and clock parameter estimation methods could benefit from such space-borne timescales.

Two basic functions of the generated space-borne timescale are real-time centimeter-level clock synchronization and the provision of a predictable time-scale reference. Based on these two functions, it is possible to autonomously update accurate broadcast clock parameters without frequent updates from the ground. Additionally, the next GNSS constellation, Kepler (Giorgi et al. 2019; Glaser et al. 2020), may use a clock-free GNSS for positioning services and generating a reference frame. Centimeter-level real-time synchronization between satellite clocks and autonomous updates to broadcast clock parameters, as proposed by this contribution, can be included in a clock-synchronized GNSS frame, in which inter-satellite clocks are synchronized before orbit determination. The corresponding benefits are included in the clock prediction method proposed in this paper, although further expansions may be possible. Other benefits of the SPBT and incorporation with other space-borne or ground-based timescales will be discussed in future work.

It should be noted that although the inter-satellite link clock offsets have advantages on clock prediction, clock offsets estimated by OTDS are more advantageous in other fields, such as real-time PPP services due to their consistency with precise orbits.

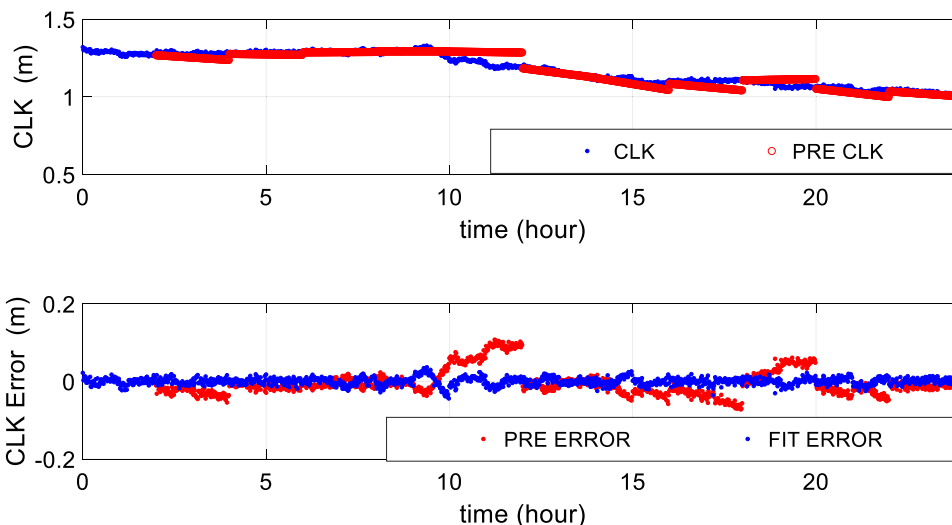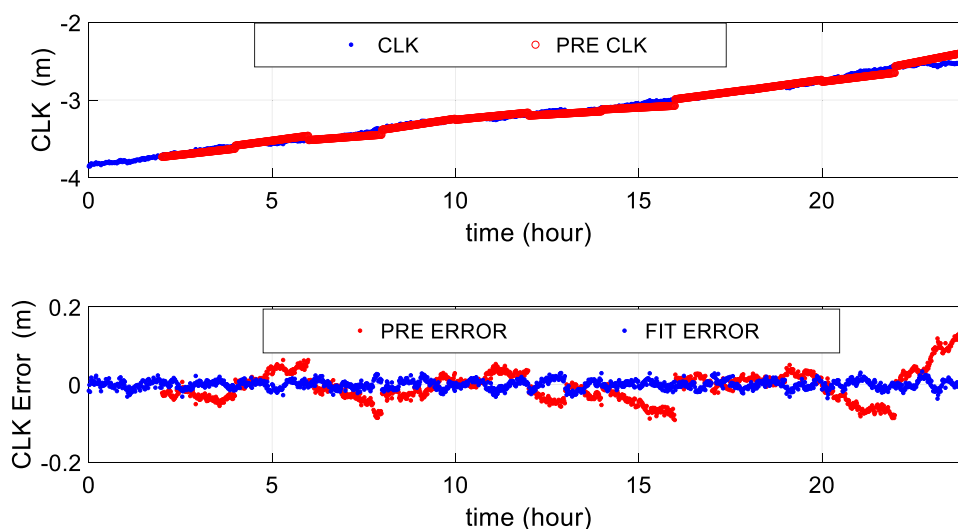**Fig. 10** Two-hour prediction
error for C40 (PHM)

Fig. 11 Two-hour prediction
error for C32 (RAFS)

Data availability The test data used in this contribution including the ISL measurements and the L-band measurements. At present, the test data are not available to the scientific community openly because they are still under test process. But they are available from the corresponding author upon request. The other data used in this contribution including precise clock provided by GFZ, which can be download from ftp://ftp.gfz-potsdam.de/.

Declarations

Conflict of interest The authors declare that they have no conflict of interest.

References

Bertiger W, Bar-Sever Y, Harvey N, Miller K, Romans L, Weiss J, Doyle L, Solorzano T, Petzinger J, Stell A (2010) Next generation GPS ground control segment (OCX) navigation design. In: Proceedings of the 23rd international technical meeting of the satellite division of the institute of navigation (ION GNSS 2010), Portland, OR, Sept. 2010, pp 964–977

Cacciapuoti L, Salomon C (2011) Atomic clock ensemble in space. J Phys Conf Ser 327:012049. https://doi.org/10.1088/1742-6596/327/1/012049

Chen J, Hu X, Tang C, Zhou S, Yang Y, Pan J, Ren H, Ma Y, Tian Q, Wu B, Yu Y (2020) SIS accuracy and service performance of the BDS-3 basic system. Sci China Phys Mech Astron 63:269511. https://doi.org/10.1007/s11433-019-1468-9

Dow JM, Neilan RE, Rizos C (2007) The international GNSS service in a changing landscape of global navigation satellite systems. J Geod 83:191–198. https://doi.org/10.1007/s00190-008-0300-3

Droz F, Mosset P, Wang Q, Rochat P, Belloni M, Gioia M, Resti A, Waller P (2009) Space passive hydrogen maser - performances and lifetime data. In: 2009 IEEE international frequency control symposium joint with the 22nd European frequency and time forum. IEEE, Besancon, France, pp 393–398. https://doi.org/10.1109/FREQ.2009.5168208

Droz F, Rochat P, Wang Q (2010) Performance overview of Space Rubidium standards *EFTF-2010 24th* European Frequency and Time Forum, Noordwijk, pp 1–6, https://doi.org/10.1109/EFTF.2010.6533702

Gao Y, Gao X, Zhang A et al (2008) The generation of new TA(NIM), which is steered by a NIM4 caesium fountain clock. Metrologia 45:S34–S37. https://doi.org/10.1088/0026-1394/45/6/s05

Ge M, Chen J, Douša J, Gendt G, Wickert J (2012) A computationally efficient approach for estimating high-rate satellite clock corrections in realtime. GPS Solut 16:9–17. https://doi.org/10.1007/s10291-011-0206-z

Giorgi G, Schmidt TD, Trainotti C et al (2019) Advanced technologies for satellite navigation and geodesy. Adv Space Res 64:1256–1273. https://doi.org/10.1016/j.asr.2019.06.010

Glaser S, Michalak G, Männel B, König R, Neumayer KH, Schuh H (2020) Reference system origin and scale realization within the future GNSS constellation "Kepler." J Geod 94:117. https://doi.org/10.1007/s00190-020-01441-0

Han C, Liu L, Cai Z, Lin Y (2021) The space–time references of BeiDou navigation satellite system. Satell Navig 2:18. https://doi.org/10.1186/s43020-021-00044-0

Hauschild A, Montenbruck O (2009) Kalman-filter-based GPS clock estimation for near real-time positioning. GPS Solut 13:173–182. https://doi.org/10.1007/s10291-008-0110-3

Jia X, Zeng T, Ruan R, Mao Y, Xiao G (2019) Atomic clock performance assessment of BeiDou-3 basic system with the noise analysis of orbit determination and time synchronization. Remote Sens. https://doi.org/10.3390/rs11242895

Johnston G, Riddell A, Hausler G (2017) The international GNSS service. In: Teunissen PJ, Montenbruck O (eds) Springer handbook of global navigation satellite systems. Springer, pp 967–982

Kouba J (2019) Relativity effects of Galileo passive hydrogen maser satellite clocks. GPS Solut 23:117. https://doi.org/10.1007/s10291-019-0910-7

Li X, Yuan Y, Huang J, Zhu Y, Wu J, Xiong Y, Li X, Zhang K (2019) Galileo and QZSS precise orbit and clock determination using new satellite metadata. J Geod 93:1123–1136. https://doi.org/10.1007/s00190-019-01230-4

Liu L, Zhu LF, Han CH, Liu XP, Li C (2009) The model of radio two-way time comparison between satellite and station and experimental analysis. Chin Astron Astrophys 33:431–439. https://doi.org/10.1016/j.chinastron.2009.09.009

Montenbruck O, Steigenberger P, Hauschild A (2015a) Broadcast versus precise ephemerides: a multi-GNSS perspective. GPS Solut 19:321–333. https://doi.org/10.1007/s10291-014-0390-8

Montenbruck O, Steigenberger P, Hugentobler U (2015b) Enhanced solar radiation pressure modeling for Galileo satellites. J Geod 89:283–297. https://doi.org/10.1007/s00190-014-0774-0

Montenbruck O, Steigenberger P, Prange L et al (2017) The multignss experiment (MGEX) of the international gnss service (IGS) – achievements, prospects and challenges. Adv Space Res 59:1671–1697. https://doi.org/10.1016/j.asr.2017.01.011

Pan J, Hu X, Zhou S, Tang C, Guo R, Zhu L, Tang G, Hu G (2018) Time synchronization of new-generation BDS satellites using inter-satellite link measurements. Adv Space Res 61:145–153. https://doi.org/10.1016/j.asr.2017.10.004

Pan J, Hu X, Zhou S, Tang C, Wang D, Yang Y, Dong W (2021) Full-ISL clock offset estimation and prediction algorithm for BDS3. GPS Solut 25:140. https://doi.org/10.1007/s10291-021-01177-0

Proia A, Bourgeolet F, d'Heeger A, Salgado G, Siccardi M, Morante Q, Varriale E, Sanchez-Gestido M, Ballereau A, Schlarmann BK (2014) Performance results of the Galileo precise timing facility. European Frequency and Time Forum (EFTF), Neuchatel, pp 463–467, https://doi.org/10.1109/EFTF.2014.7331536

Qin W, Wei P, Yang X, Ren X (2018) Analysis of inuence factors on autonomous time-maintenance algorithm of navigation satellites. Acta Astronom Sinica 059(001):11–23. https://doi.org/10.15940/j.cnki.0001-5245.2018.01.002

Qin W, Ge Y, Wei P, Dai P, Yang X (2019) Assessment of the bds-3 onboard clocks and their impact on the ppp time transfer performance. Measurement 153:107356

Senior KL, Coleman MJ (2017) The next generation GPS time. Navigation 64:411–426. https://doi.org/10.1002/navi.208

Steigenberger P, Montenbruck O (2016) Galileo status: orbits, clocks, and positioning. GPS Solut 21:319–331. https://doi.org/10.1007/s10291-016-0566-5

Steigenberger P, Montenbruck O (2019) Consistency of MGEX orbit and clock products. Engineering 6:898–903. https://doi.org/10.1016/j.eng.2019.12.005

Tang C, Hu X, Zhou S, Guo R, He F, Liu L, Zhu L, Li X, Wu S, Zhao G, Yu Y, Cao Y (2016) Improvement of orbit determination accuracy for Beidou navigation satellite system with two-way satellite time frequency transfer. Adv Space Res 58:1390–1400. https://doi.org/10.1016/j.asr.2016.06.007

Tang C, Hu X, Zhou S, Liu L, Pan J, Chen L, Guo R, Zhu L, Hu G, Li X, He F, Chang Z (2018) Initial results of centralized autonomous orbit determination of the new-generation BDS satellites with inter-satellite link measurements. J Geod 92:1155–1169. https://doi.org/10.1007/s00190-018-1113-7

Wang H, Chen Z, Zheng J, Chu H (2011) A new algorithm for onboard autonomous orbit determination of navigation satellites. J Navig 64:S162–S179. https://doi.org/10.1017/s0373463311000397

Wang YP, Lv ZP, Li LY, Zhai SF (2017b) Analysis of the long-term performance of GPS BLOCK IIF satellite atomic clocks. Acta Astron Sin 58:20

Wang H, Xie J, Zhuang J, Wang Z (2017a) Performance analysis and progress of inter-satellite-link of Beidou system. In: Proceedings of the 30th international technical meeting of the satellite division of the institute of navigation (ION GNSS+ 2017a). Institute of Navigation, Portland, Oregon, pp 1178–1185 https://doi.org/10.33012/2017.15204

Warren DLM, Raquet JF (2003) Broadcast vs. precise GPS ephemerides: a historical perspective. GPS Solut 7:151–156. https://doi.org/10.1007/s10291-003-0065-3

Weiss M, Weissert T (1991) AT2, a new time scale algorithm: AT1 plus frequency variance. Metrologia 28:65–74. https://doi.org/10.1088/0026-1394/28/2/002

Wu Z, Zhou S, Hu X, Liu L, Shuai T, Xie Y, Tang C, Pan J, Zhu L, Chang Z (2018) Performance of the BDS3 experimental satellite passive hydrogen maser. GPS Solut 22:44. https://doi.org/10.1007/s10291-018-0706-1

Yang J, Tang C, Song Y, Hu X, Zhou S, Chang Z (2021) Analysis of signal-in-space ranging error of GNSS navigation message(in Chinese). SciSin-Phys Mech Astron. https://doi.org/10.1360/SSPMA-2020-0227

Zhou S, Hu X, Liu L, Guo R, Zhu L, Chang Z, Tang C, Gong X, Li R, Yu Y (2016) Applications of two-way satellite time and frequency transfer in the BeiDou navigation satellite system. Sci China Phys Mech Astron 59:109511. https://doi.org/10.1007/s11433-016-0185-6

Zhou W, Ruan R, Jia X, Jin R (2020) BDS-3 onboard atomic clock performance evaluation. In: Sun J, Yang C, Xie J (eds) China satellite navigation conference (CSNC) 2020 proceedings, vol III. Springer, Singapore, pp 134–143